Received: 21 December 2021 | Revised: 6 April 2022 | Accepted: 6 April 2022

DOI: 10.1002/asl.1096

RESEARCH ARTICLE

Atmospheric Science Letters RMetS

Interannual variability of spring fire in southern Nepal

Kalpana Hamal[1,2] | **Shravan Kumar Ghimire**[2,3] | **Arbindra Khadka**[4,5,6] | **Binod Dawadi**[6,7] | **Shankar Sharma**[6]

[1]International Center for Climate and Environment Sciences, Institute of Atmospheric Physics, Chinese Academy of Sciences, Beijing, China

[2]University of Chinese Academy of Sciences, Beijing, China

[3]Institute of Mountain Hazards and Environment, Chinese Academy of Sciences, Chengdu, China

[4]University of Grenoble Alpes, CNRS, IRD, IGE, Grenoble, France

[5]International Centre for Integrated Mountain Development, Lalitpur, Nepal

[6]Central Department of Hydrology and Meteorology, Tribhuvan University, Kathmandu, Nepal

[7]Kathmandu Center for Research and Education, Chinese Academy of Sciences–Tribhuvan University, Kathmandu, Nepal

Correspondence
Shankar Sharma, Central Department of Hydrology and Meteorology, Tribhuvan University, Kathmandu 44613, Nepal.
Email: sharma.sh969@gmail.com

Funding information
This research did not receive any internal or external funding. This research is conducted independently by the authors as a part of their research and study. The organization and institution mentioned in the study have no role in the design and funding of the study.

Abstract

Nepal is highly vulnerable to climate change with increased fire occurrences and fire burned areas in recent years; therefore, we accessed the climatic drivers for its variability using fire burned areas product of Moderate Resolution Imaging Spectroradiometer (MODIS) from 2001 and 2020. The peak fire burned areas were observed in the spring season (~91%) from March to May, especially higher in the lowlands of the western and central parts. At the interannual timescale, low precipitation, humidity, soil moisture, and high temperature supported the existence of spring fire. Combining these factors induces drought conditions, enhancing evapotranspiration from vegetation and providing more combustible fuels. Furthermore, the El Niño phase in the central-eastern Pacific Ocean is related to the weakened westerly moisture transport and moisture divergence that creates dry and warm conditions leading to increased fire activities. Thus, this study could be helpful for preparedness, management, and policy-making to limit the multi-dimensional losses in the ecosystem and society due to fire.

KEYWORDS

burned areas, ENSO, fire, Nepal, spring season

1 | INTRODUCTION

The central Himalayan country, Nepal, is bordered between China and India, with altitudinal variation from the Indo-Gangetic plains to the high Himalayas. The topographical complexity of the country has provided diverse climatic belts, biodiversity, and epic landforms (Upreti, 2001). However, the complex topography has made the country prone to natural disasters such as earthquakes, landslides, floods, fires, and thunderstorms (Chitrakar et al., 2007; Dhakal, 2015). Fire incidents account for the highest number of recorded natural disasters in Nepal, causing significant loss

of life and property, biodiversity, and natural resources (MoHA, 2018). The primary reasons behind the fire in Nepal are uncontrolled burning for regenerating new shoots, straw burning, negligence, discarded cigarettes, lightning, electrical short circuit, and enhanced climatic conditions (BBC, 2021; Skamarock, 2008). These forest fires are becoming the cause of the rising air pollution in the different cities of Nepal (Zhongming et al., 2021), causing health problems, such as burning eyes, a runny nose, and chronic heart and lung disease. Furthermore, it releases significant greenhouse gases and aerosols that can affect the earth's radiative budget and air quality at local and regional scales (Lasko & Vadrevu, 2018; Vadrevu, 2016; Wang et al., 2007). Hence, the fire hazards could have unprecedented impacts on livelihood, ecosystems, and weather systems.

In terms of fire hotspot area, Nepal ranked in the third position (29.5%) out of seven South Asian countries after India (32.2%) and Bangladesh (34.2%) (Reddy et al., 2019). The forest fire mainly occurs in the spring (March–May) season; moreover, it was found that 18 out of the 75 districts were at high risk (Matin et al., 2017). The Moderate Resolution Imaging Spectroradiometer (MODIS) instrument on National Aeronautical Space Agency's Aqua satellite captured on April 24, 2012, showed numerous burned areas throughout the country (https://earthobservatory.nasa.gov/images/77784/fires-in-nepal). Similarly, Parajuli et al. (2015) found an average of 2159 fire counts per year during 2000 to 2013, with the highest in 2012. The situation was worst in 2016 when the fire occurrences and burned areas were 33% and 42% more compared to the annual average of 2000–2015 (Bhujel et al., 2017). Therefore, there has been an urge for spatial–temporal analysis of the fire burned areas until recent years to make an effective management plan and policy.

The majority of the forest fire occurrences in Nepal are considered anthropogenic driven (Matin et al., 2017); however, the climates factors (e.g., precipitation, temperature, humidity) further exacerbated the possibility of ignition and spread (Fang et al., 2021; Tang et al., 2021). The climatic influence on the fire regime is essential for establishing a baseline to understand the relationship that determines the spatial and temporal variations of fire occurrences and burned areas (Eskandari et al., 2020). The prolonged precipitation deficit and the warmer temperature have a higher risk of fire occurrences and spread (Curic & Zivanovic, 2013). For instance, in southeastern China, the leading cause of wildfires is decreased precipitation and increased diurnal temperature range, whereas this combination produces high combustible fuel to fire activity (Fang et al., 2021). Similarly, Yi et al. (2017) found the simultaneity relationship between the precipitation variation and burn area over China. Further, the dry soil moisture anomalies precede the fire by providing the suitable ignition condition and flammability compared to the wet soil moisture anomalies (Sungmin et al., 2020). Generally, when the surface wetness deviation exceeded +5%, a larger burn area was not detected in Siberia, indicating that wet soil moisture condition limits the extent of the burned areas (Bartsch et al., 2009). Furthermore, the high availability of relative humidity limits fire occurrences, as the significant negative relationship observed between fire occurrences and relative humidity (Eskandari et al., 2020). Therefore, we focused to analyzes the impacts of the different climatic variables on the fire burned areas over Nepal.

The Indo-Pacific sea surface temperature (SST) anomalies are related to global fire occurrences (Dong et al., 2021; Fang et al., 2021; Mariani et al., 2016; Wang & Cai, 2020). The El Niño Southern Oscillation (ENSO) is one of the natural factors for fire occurrences (Burton et al., 2020; Siegert et al., 2001; Yang et al., 2021), accounting for one-third of the total predictable global burned areas (Chen et al., 2016). For instance, the El Niño reduced the precipitation and terrestrial water storage in pan-tropical forests by 133%, enhancing the fire events (Chen et al., 2017). Similarly, the dipole pattern of the wildfire activities between southwestern and southeastern China was modulated by ENSO, varying the strength of precipitation and wind anomalies in the fire season (Fang et al., 2021). It also increased hot and dry conditions in fire-prone regions (Burton et al., 2020). Furthermore, the 2-year consecutive occurrence of Indian Ocean Dipole and Central Pacific El Niño contributed to unprecedented severe 2019–2020 Australian bushfires (Wang & Cai, 2020). It also found that Indian SST plays an essential role in the 2019 Amazonia fires (Dong et al., 2021). However, there is a lack of understanding of the fire regime (burned areas) and its large-scale climatic drivers in Nepal.

Overall, this study investigates answering three research questions: (a) How the fire burned areas vary across the country over the last 20 years (2001–2020); (b) How the burned areas are related to the climatic variables; and (c) How the burned areas are related with the SST over the Indo-Pacific Ocean.

2 | MATERIAL AND METHODS

2.1 | Study area

Nepal is located in the central part of the Himalayas between 80°3′30.43″– 88°12′5.46″E longitude and 26°20′52.72″–30°28′23.37″N latitude (Figure 1a). Due to the high gradient from the plains of ~60 m in the south to 8848.86 m a.s.l. in the north, the country features a complex topography,

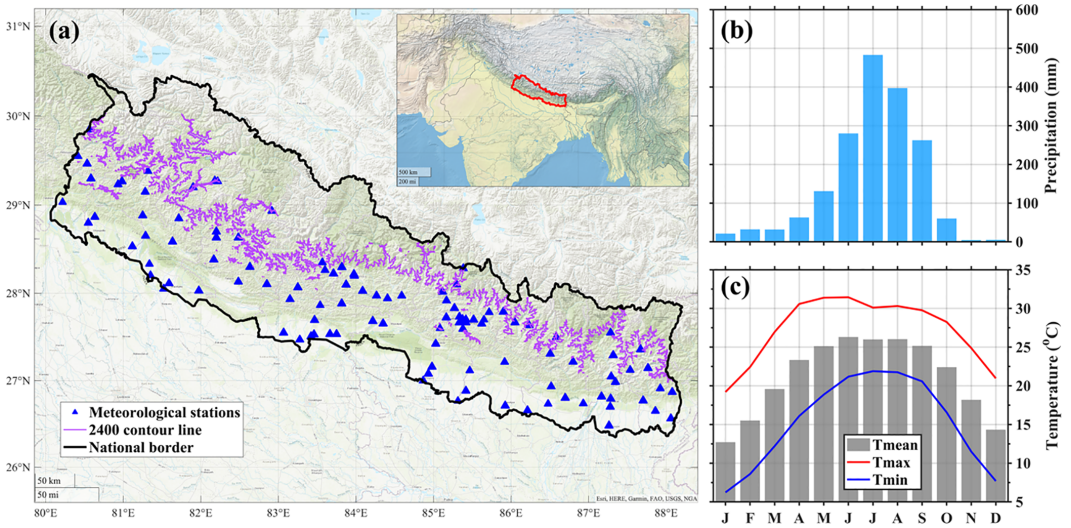

FIGURE 1 (a) Study area, Nepal, and selected meteorological stations over southern Nepal. The monthly cycle of (b) average precipitation and (c) surface air temperature of southern Nepal during 2001 to 2020. The magenta color and inset map in (a) show the 2400 m elevation contour and country's position in the south Asian region, respectively

unique landscapes, diverse ecosystems, climatic belts, and weather patterns. Typically, four seasons in the country are; spring (March–May), summer (June–September), autumn (October–November), and winter (December–February) (Nayava, 1980). The spring, autumn, and winter are dry seasons, whereas summer receives more than 80% of the total precipitation (Sharma et al., 2020a). The spring has westerly disturbed and localized precipitation with hot and dry temperatures, whereas a humid climate with widespread precipitation characterizes the summer season (DHM, 2017). The post-monsoon and winter are dry and cold, contributing about 4% and 3% of annual precipitation, respectively (Sharma et al., 2020b). The precipitation in winter is primarily generated by the westerly wind system and is more prominent in the western region of the country (Hamal et al., 2020). The surface air temperature and vegetation density in Nepal decrease with increasing latitude and altitude (Carpenter, 2005). Furthermore, southern Nepal, mainly tropical to temperate region, experiences a heavy fall of leaves in the summer season, providing a favorable environment for fire activities (Matin et al., 2017; Qadir et al., 2021). Therefore, we choose only southern Nepal (tropical to the temperate region; up to 2400 m a.s.l.) for the present study (Figure 1a).

2.2 | Datasets

2.2.1 | Observation datasets

For the observed climatology, we have initially collected daily precipitation and temperature records from 160 stations from the Department of Hydrology and Meteorology (DHM), Government of Nepal (www.dhm.gov.np). The selected in situ datasets do not feature regular observation, and quality control is applied for data homogeneity and handling missing values. To do this, we have selected those stations featuring more than 80% daily time series of precipitation and surface air temperature from 2001 to 2020. After the quality control, 109 stations located between tropical and temperate regions (below 2400 m a.s.l.) were selected for the current study (Figure 1a). Furthermore, monthly, seasonal and annual data are generated by averaging daily precipitation and temperature.

2.2.2 | Fire data

We used MODIS (aqua and terra combined) Fire_cci version 5.1 burned area products (Lizundia-Loiola et al., 2020). Fire_cci is one of the Essential Climate Variables (Fire disturbance) under the European Space Agency's Climate Change Initiative (CCI). The latest version, that is, FireCCI5.1, is the improvement of the previous version (FireCCI41), available from 2001 to 2020 (last accessed on Feb 2021). It was generated by combining spectral information from MODIS at 250-m resolution and thermal information from the MODIS active fire products. The daily MODIS Surface Reflectance product (MOD09GQ) collection of six images, the Land Cover Project of ESA CCI, and the MODIS Global Monthly Fire Location Product (MCD14ML collection 6) are used as the primary inputs to derive the burned areas product

(Lizundia-Loiola et al., 2020). MODIS burned areas product has the most extended time series with the most improved algorithm and the best validation results. Therefore, we have downloaded the gridded product (0.25 km spatial resolution) between 2001 and 2020 from https://geogra.uah.es/fire_cci/firecci51.php(accessed on Feb 2021). For further information on the characteristics and variables of the dataset can be acquired from https://admin.climate.esa.int/media/documents/Fire_cci_D4.2.1_PUG-MODIS_v1.1.pdf. In addition, we have also used MODIS (aqua and terra combined) version 6 fire detection products (MCD14ML) from the University of Maryland (available at: https://earthdata.nasa.gov/firms).

2.2.3 | ERA5datasets

We have used monthly datasets of the precipitation (PRE), surface air temperature (SAT), wind, soil moisture (SM) at the surface level (0–7 cm), relative humidity (RH) at 1000 hPa, vertically integrated moisture flux divergence (VIMD), vertically integrated moisture flux (VIMF), geopotential height (GPH) at 500 hPa and SST from ERA5 between 2001 and 2020, with 0.25° × 0.25° spatial resolution (C3S, 2017). Recently, Sharma et al. (2020a) and Chen et al. (2021) validated the ERA5 precipitation product using gauge observed datasets revealing ERA5 as a good alternative for precipitation monitoring over Nepal. Moreover, several previous studies have successfully applied these ERA5 products to analyze oceanic and atmospheric circulation related to precipitation and drought (Hamal et al., 2020; Hamal et al., 2021; Sharma et al., 2020a). The NINO 3.4 is calculated as the average SST anomaly over the Central Pacific Ocean (CP), ranging from 5°N to 5°S and 170°W to 120°W. In addition, NINO3 is the average SST over the Eastern Pacific Ocean (EP): 5°N to 5°S and 150°W to 90°W.

2.2.4 | Vegetation Health Index

The vegetation health index (VHI) measures relative vegetation health that can be derived using a factor sum of the Vegetation Condition Index (VCI) and Temperature Condition Index (TCI) (Kogan, 2001). VCI is derived from the Normalized Vegetation Index and TCI from the land surface temperature.

$$\mathrm{VHI} = \propto .\mathrm{VCI} + (1 - \propto).\mathrm{TCI} \quad (1)$$

where, $\propto$ is a constant of 0.05.

In this study, the monthly VHI of March–May from 2001 to 2020 was evaluated in Google Earth Engine (GEE) platform using the earth observation dataset produced by the Food and Agriculture Organization (FAO) of the United Nations (https://data.apps.fao.org/map/catalog/srv/eng/catalog.search#/metadata/1eb5883d-05c6-427f-bbf7-8465bfb7069c). FAO has used 1 km resolution data of National Oceanic and Atmospheric Administration —Advanced Very High-Resolution Radiometer (NOAA-AVHRR) and Meteorological Operational—Advanced Very High-Resolution Radiometer (METOP-AVHRR) from 2001 to 2006 and 2007 to 2020, respectively to generate VCI and TCI.

2.3 | Methodology

2.3.1 | Correlation analysis

The correlation analysis quantifies the direction and strength of the linear association between the variables giving the positive or negative relation (Stockwell, 2008). We performed a correlation analysis of spring fire burned areas with the climatic variables, SST pattern and their indices, and atmospheric circulation from 2001 to 2020 using the two-tailed Student's *t*-test at different confidence levels (at 90%, 95%, and 99%). Note that all datasets were detrended before passing through the correlation analysis to remove the existing trend.

2.3.2 | Drought Index

We have used Standardized Potential Evapotranspiration Index (SPEI), which uses precipitation (P_i) and potential evapotranspiration (PET_i) to calculate water balance (D_i) (Equation 2). The precise method for calculating SPEI is given by Vicente-Serrano et al. (2010). The PET is calculated using the Thornthwaite method, which requires only the mean temperature (Thornthwaite, 1948). The D_i is fitted through the log-logistic distribution function, and then SPEI at different timescales is obtained. For the current study, we have used SPEI3-May, a spring drought index that uses precipitation and temperature from March to May. The threshold for the drought determination is SPEI ≤ −1.

$$D_i = P_i - \mathrm{PET}_i,\ i = 1,2,3,\ ...,n \quad (2)$$

2.3.3 | Singular value decomposition analysis

Singular value decomposition (SVD) analysis has been used in this study to examine the coupled pattern of fire-

burned areas and SST departure during the spring season from 2001 to 2020. It is widely used because of its simple implementation and strength to extract the results of the coupled signals (Fang et al., 2021; Mishra et al., 2012; Riaz & Iqbal, 2017). The details of SVD analysis and its theoretical aspect can be found in (Bretherton et al., 1992). The SVD analysis is performed on the burned area and SST over the Indo-Pacific Ocean; then, the first homogeneous leading mode is chosen to explain maximum covariance.

3 | RESULT AND DISCUSSION

3.1 | Interannual variation

Most of the forests and agricultural land of Nepal are located between tropical and temperate regions; therefore, the analysis of burned areas is focused below the 2400 m elevation range. The seasonal cycle of the average monthly fire-burned areas over southern Nepal during 2001 to 2020 is shown in Figure 2a. The result shows that 91.2% of the fire-burned areas during the spring, followed by the winter (6.3%), summer (2.1%), and autumn (0.4%) season. The fire season starts from January to May, with the peak in April and decreases from July as the monsoon progresses. During the fire season, southern Nepal receives ~13% of the total precipitation with warm temperatures (Figures 1b and c); these climatic factors might have exacerbated the fire events. In contrast, the high amount of precipitation in the summer (Figure 1b) creates wet conditions that might cease the fire activity, resulting in line with Fang et al. (2021) and Bhardwaj et al. (2016).

As the fire burned areas are highest in the spring season, the spatial distribution of the average spring burned areas are presented in Figure 2b. The southern lowlands are covered with dense forest and agricultural land; the large burned areas were observed in the lowlands of the western and central parts. During the past two decades, spring fire-burned areas were recorded at an average of 5.5 km^2 with a total of ~46,046 km^2. It has also been observed that the average fire burned areas are significantly increasing at a rate of 0.26 km^2 $year^{-1}$ ($p < 0.1$). Similarly, an increasing trend of fire events was observed in all South Asian countries, where Nepal ranked third with a total of 32,018 annual fire counts between 2012 and 2016 (Vadrevu et al., 2019). The year 2015 had the lowest burned area of 218 km^2 and standardized anomalies <-1; however, the following year, that is, 2016, had unusually high-burned areas reaching 7532 km^2 and standardized anomalies exceeding +3. Furthermore, 6466 and 3352 fire counts were observed over southern Nepal in 2016 and 2019, showing high fire counts related to increased burned areas (Figure S1). Similarly, MoHA (2018) has also reported the fire incidence (1856 events) in 2015/2016, which outnumber lighting (299), landslide (290), flood (244), and heavy rainfall (188). In the meantime, Asian regions also experienced high fire occurrences (Burton et al., 2020), causing a significant ecological and socio-economic impact.

3.2 | Fire-climate relationship

We further investigated the influence of the climatic factors (e.g., PRE, SAT, SM, and RH) on the fire burned

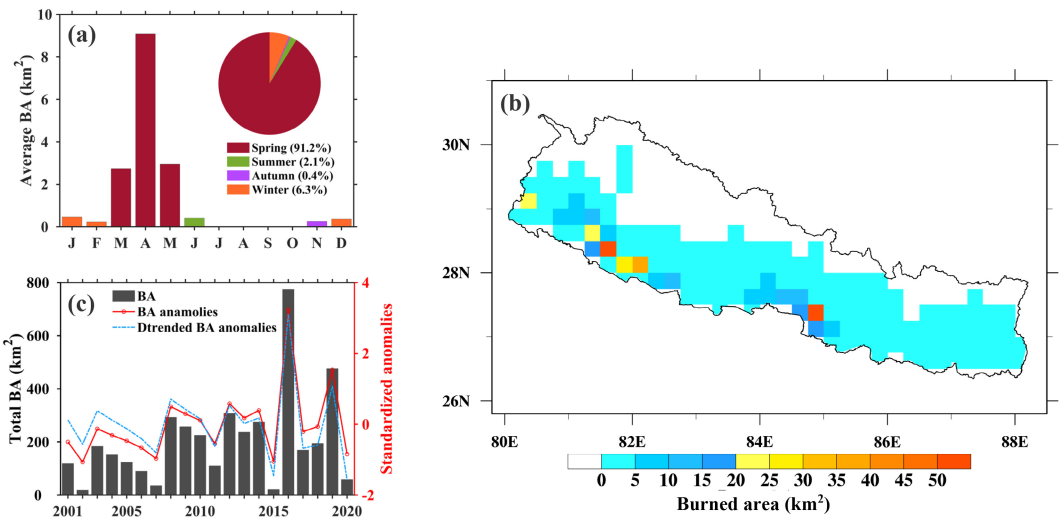

FIGURE 2 (a) Seasonal cycle, (b) spatial distribution, and (c) yearly variation of total and standardized anomalies of the spring fire burned areas (BA, km^2) over southern Nepal between 2001 and 2020

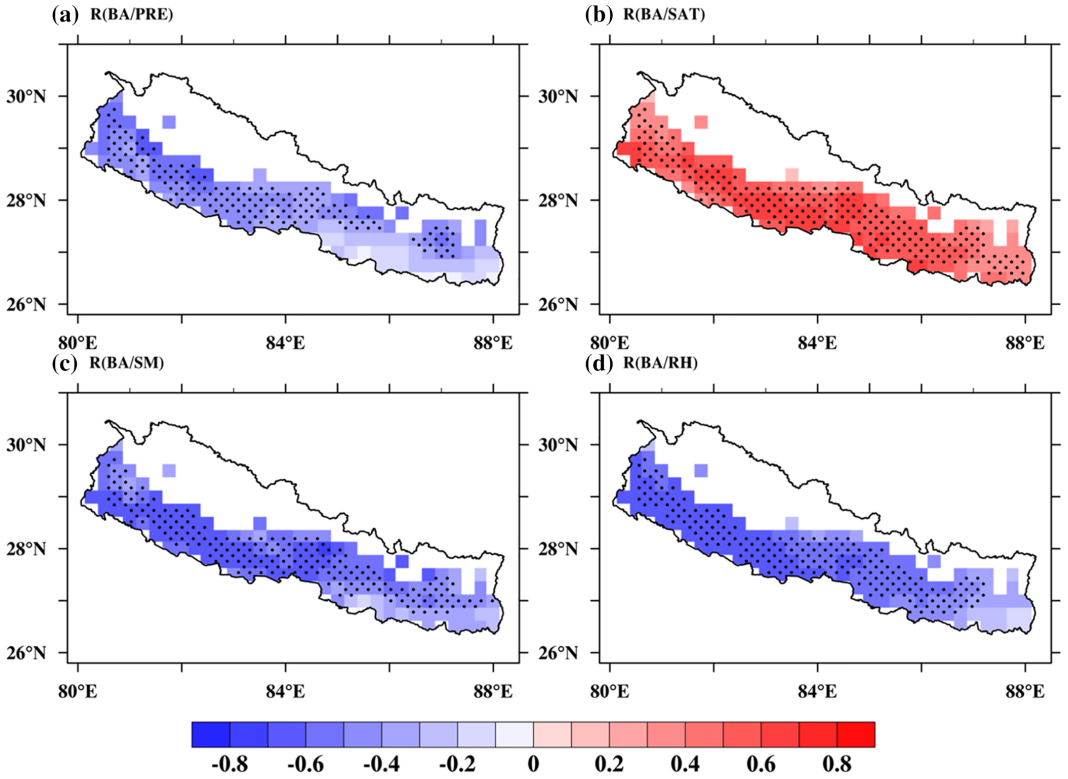

FIGURE 3 The correlation (R) of fire burned areas (BA, km^2) with (a) precipitation (PRE, mm $month^{-1}$), (b) surface air temperature (SAT,°C), (c) soil moisture (SM, m^3 m^{-3}) at the surface level (0–7 cm) and (d) relative humidity (RH, %) at 1000 hPa during the spring season from 2001 to 2020 using ERA5 datasets. The black dots represent the significant correlation at a 90% confidence level

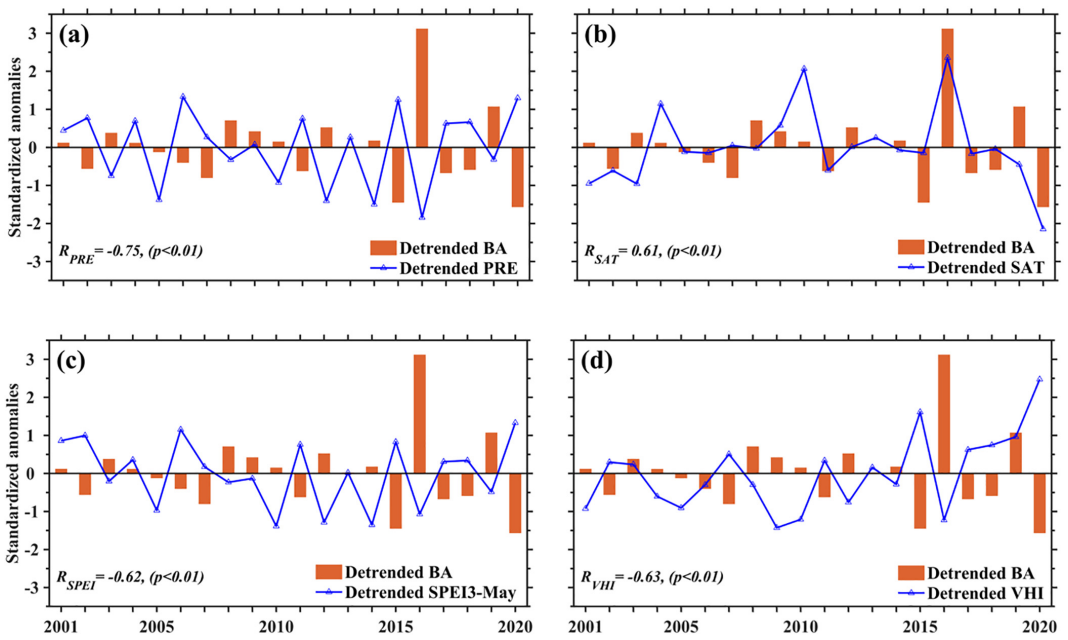

FIGURE 4 Temporal correlation (R) of fire burned areas (BA, km^2) with (a) observed precipitation (PRE, mm $month^{-1}$), (b) observed surface air temperature (SAT, °C), (c) drought index (SPEI3-May), and (d) vegetation health index (VHI) during spring season between 2001 and 2020

areas over southern Nepal during the peak fire season (Figure 3). A significant negative correlation was observed between fire burned areas and ERA5 precipitation over the lowlands of the western and central region and mid-hills of the eastern region (Figure 3a). Similarly, the area average interannual time

series of the burned areas and in situ precipitation shows a significant negative correlation ($R = -0.75$, $p < 0.01$; Figure 4a). During the fire season, the long dry spells can further exacerbate the fire burned areas; for example, the fire count and burned areas were higher than normal in the precipitation deficit year, that is, 2012, 2016, and 2019 (Hamal et al., 2020; Sharma et al., 2021). Moreover, a strong positive correlation of fire burned areas with the ERA5, and in situ surface air temperature (Figures 3b and 4b) indicates that high temperature can result in the dry condition that can initiate fire activities (Fang et al., 2021; Kim et al., 2020; Tang et al., 2021).

Furthermore, the availability of soil moisture and relative humidity can directly impact fire intensity and distribution (Bartsch et al., 2009; Eskandari et al., 2020; Sungmin et al., 2020). The strong negative correlation in Figures 3c, d further confirms that the low soil moisture and relative humidity can create dry conditions for the surface and fuel. Such dry conditions lead to high evapotranspiration from vegetation, triggering the fire intensity, and spread (Moinuddin et al., 2021; Sungmin et al., 2020).

As precipitation (temperature) shows a negative (positive) correlation with fire burned areas, therefore; the correlation between fire burned areas and drought index was performed in Figure 4c. We used area-averaged in situ precipitation and temperature during the fire season to calculate the SPEI3 and then selected the SPEI3-May to represent the spring drought index (Figure 4c), which shows the significant negative correlation ($R = -0.62$, $p < 0.01$) with burned areas. The fire years: 2012, 2016, and 2019 with standardized anomalies >0.5 are related to the spring drought, indicating the fire burned areas increased in response to drought (Littell et al., 2016). The low-precipitation, soil moisture, relative humidity, and high temperature produce drought condition that negatively affects vegetation health. Likewise, the health of the vegetation is negatively affected by the fire activity ($R = -0.63$, $p < 0.01$; Figure 4d). For instance, the major forest ecosystem affected by the fire is sal and mixed broad-leaved, Chir pine, and Schima-Castanopsis forest in southern Nepal (MENRIS-ICIMOD, 2008). During March and April, warm temperature leads to high evapotranspiration, leading to loss of moisture from vegetation producing combustible fuel (dry wood, logs, dead leaves, stumps, dry grass, and weeds), increasing the risk of fire activity and spread (Johnson & Miyanishi, 2001).

3.3 | Fire-oceanic and atmospheric relationships

We performed an SVD analysis between the spring fire burned areas and the SST field, accounting for 54.1% of

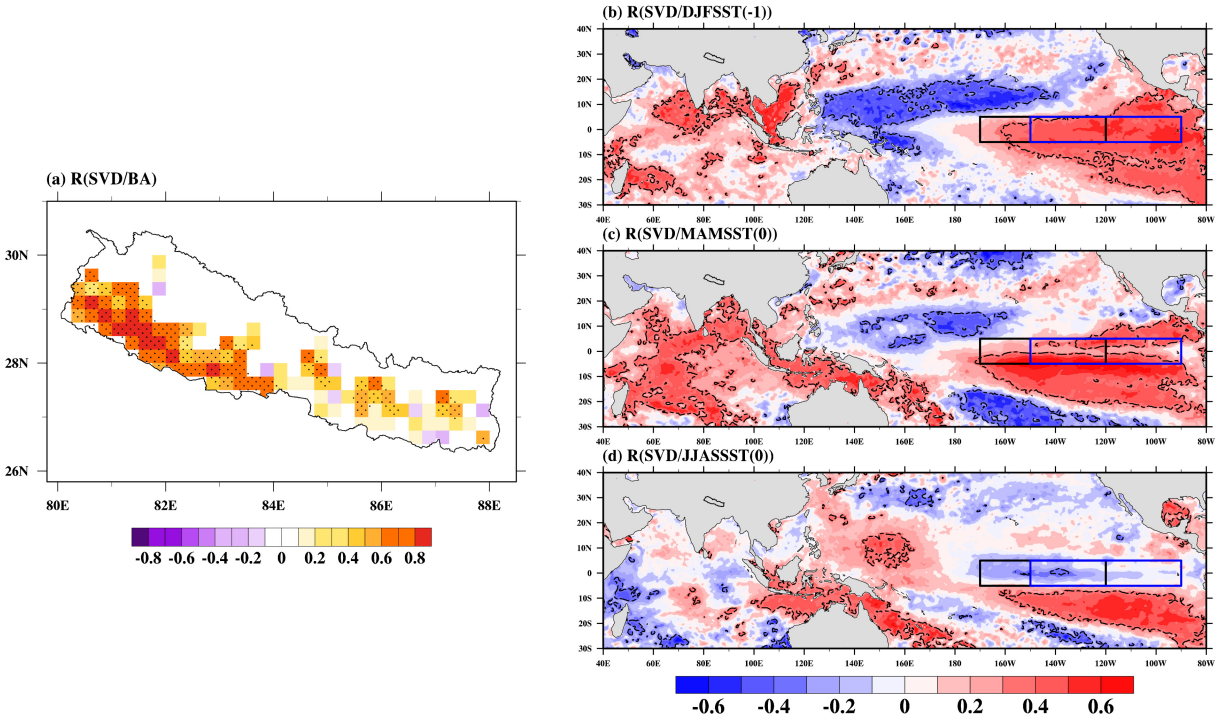

FIGURE 5 The correlation (R) of the first leading singular value decomposition (SVD) with (a) fire burned areas (BA, km^2) and sea surface temperature (SST, °C) during (b) preceding winter (DJFSST[−1]), (c) concurrent spring (MAMSST[0]), and (d) summer (JJASSST [0]). The black dots and contour represent significant correlations at a 90% confidence level. The black and blue box represents the NINO3.4 and NINO3 regions, respectively

their total covariance in the first mode (Figure 5). The first leading SVD mode confirmed significant burned areas in southern Nepal due to the SST variation in the Indo-Pacific Ocean (Figure 5a). Therefore, the first leading SVD mode was correlated with SST anomalies over the Indo-Pacific Ocean from the preceding winter to the following summer, presented in Figure 5b-d. The strong eastern ENSO type was observed in the prior winter, characterized by a positive SST anomaly in the EP that extends up to 160°W in the CP region (Figure 5b). In the corresponding fire season, the ENSO moves toward 170°W in the CP region (Figure 5c). The basin-wide Indian Ocean warming was observed; El Niño induces this condition in the developing and decaying years (Chowdary & Gnanaseelan, 2007; Zhou et al., 2019). The El Niño in the central-eastern Pacific Ocean had a transition from positive to negative in the summer; no significant relation was observed between fire burned areas and SST (Figure 5d). The result indicates that ENSO in the developing and decaying phase significantly influences the fire burned areas in southern Nepal.

We further confirmed the relationship of the ENSO at EP (NINO3) and CP (NINO3.4) with the leading mode of SVD in Figure 6. A significant positive correlation was observed between the first leading SVD mode and both ENSO types, whereas the EP type ENSO (Figure 6b) has more substantial impacts than CP type ENSO (Figure 6a). Furthermore, we also compared the high fire burned areas in 2016 and 2019 with ENSO. Year 2015/2016 has extreme El Niño conditions, that is, warm standardized anomalies of +2.3 in the preceding winter that decays to +1.9 in the corresponding spring over the CP type. Similarly, +2.6 and +2 standardized anomalies in the preceding winter and corresponding spring were observed over the EP type. Likewise, the El Niño conditions in the EP resulted in the 2015/2016 global fire (Burton et al., 2020; Chylek et al., 2018). In 2019, the SST anomalies in the central-eastern tropical Pacific Ocean indicated a weak El Niño event in the preceding winter; however, it showed a moderate El Niño event during the corresponding season. It was forecasted that moderate El Niño conditions would persist till spring, and gradual decay to near-neutral or slightly positive anomalies would be obtained till mid-summer (see Figure 7, https://judithcurry.com/2019/04/04/2019-enso-forecast/v). Similar to studies of southeastern China (Fang et al., 2021) and southeast Australia (Mariani et al., 2016), our findings also indicated the high fire burned areas in southern Nepal are observed during the developing and decaying El Niño phases over the central-eastern Pacific Ocean

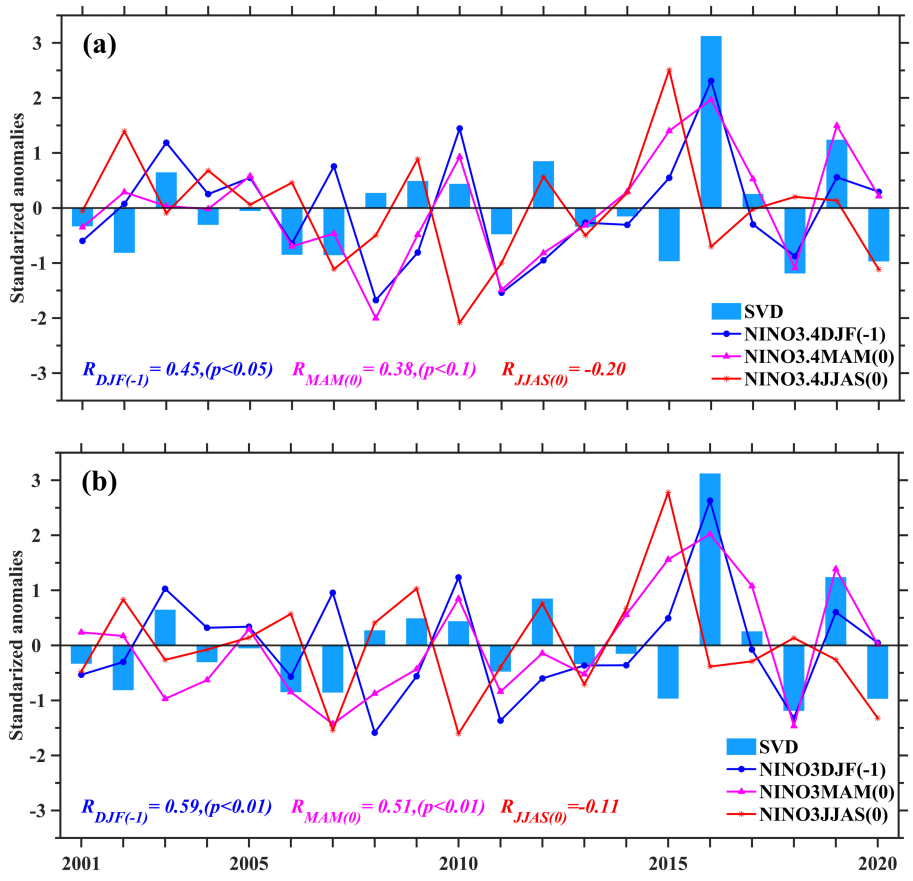

FIGURE 6 Temporal correlation (R) of the first leading SVD mode with (a) NINO3.4 and (b) NINO3 at preceding winter (DJFSST[−1]), concurrent spring (MAMSST[0]), and summer (JJASSST[0])

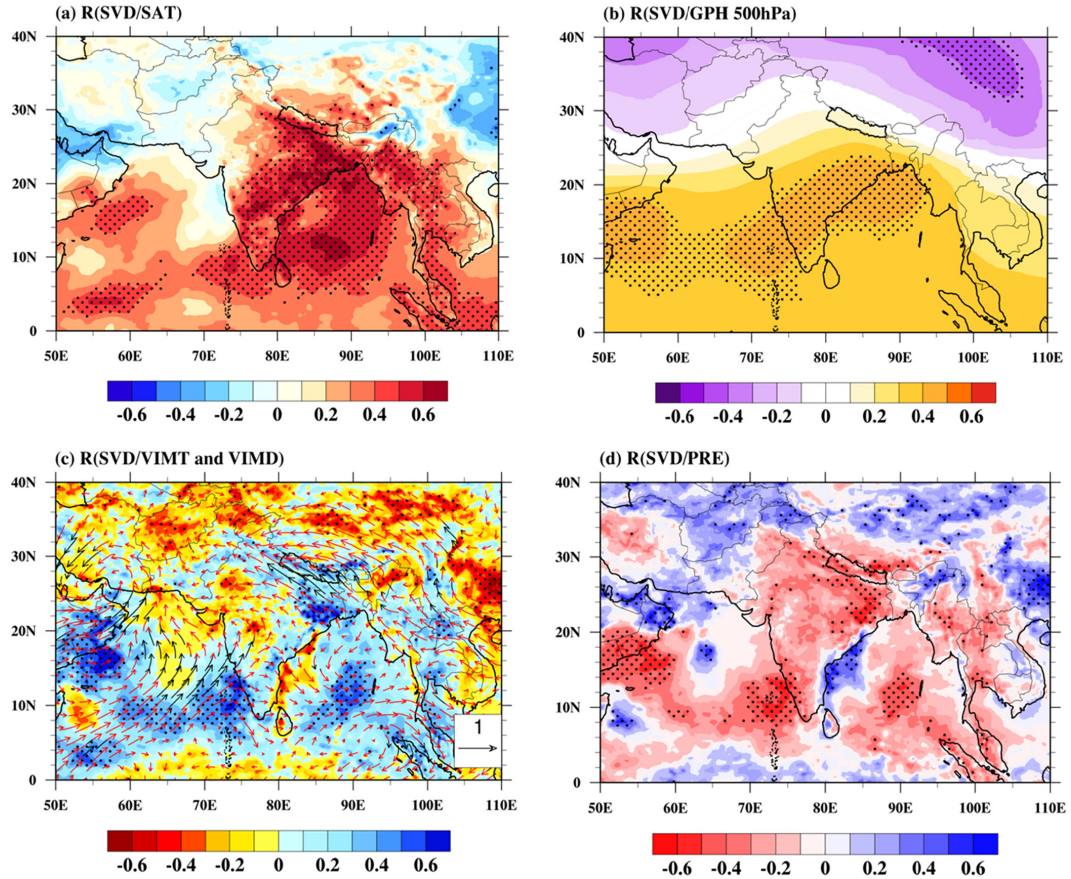

FIGURE 7 The correlation (R) of the first leading SVD mode with (a) surface air temperature (SAT,°C), (b) geopotential height (GPH, $m^2\ s^{-2}$) at 500 hPa, (c) vertically integrated moisture flux divergence (VIMD, 10^{-5} kg $m^{-1}\ s^{-1}$, contour, negative and positive correlation indicate moisture convergence and divergence, respectively) and vertically integrated moisture transport (VIMT, kg $m^{-1}\ s^{-}1$, vectors) and (d) precipitation (PRE, mm $month^{-1}$). The black dots and red vectors denote that the correlations are significant at a 90% confidence level

(Figure 6). In addition, Wang and Cai (2020) found the Indian Ocean SST's role in fire occurrences; for instance, the two-year consecutive (2018 and 2019) positive Indian Ocean Dipole events in conjunction with the consecutive (2018 and 2019) El Niño events were the primary reason for the recent 2019/2020 Australian catastrophic bushfires.

Further, to confirm the influence of the ENSO on the first mode of SVD, we correlated the leading mode of SVD with the SAT, GPH at 500 hPa, VIMT, VIMD, and PRE (Figure 7). During the El Niño phase, a higher temperature was observed over South Asia and the Bay of Bengal region, leading to dry and warm conditions (Figure 7a). This extremely high temperature over the study region will enhance the risk of fire activity. Furthermore, the higher-than-average GPH was extended from the Arabian Sea, passing the Indian peninsula to the Bay of Bengal (Figure 7b), indicating the weakened climatical trough and El Niño's influence on the atmospheric circulation (Fang et al., 2021; Sharma et al., 2020a). Similarly, the positive GPH anomalies contributed to wildfires in northeast China (Zhao & Liu, 2019). Such GPH patterns weaken the moisture transport by creating warm and dry conditions, which is supported by a significant moisture divergence and weakened moisture flux in northern India and the study region (Figure 7c).

The westerly moisture flux is dominant over northern India, Nepal, and Bangladesh in the spring season ([Tanoue et al., 2018]; see Figure 5); moisture transport is mainly from the Arabian Sea to the Indian subcontinent. Similarly, the moisture source to the study region from the Bay of Bengal is nearly cutoff with more prevailing westerly trajectories (Perry et al., 2020). The results show that moisture convergence is high over the northern Arabian Sea; however, the westerly moisture transport is suppressed (Figure 7c). The northeasterly moisture transport is initiated toward northern India and Nepal with anomalous anticyclonic circulation and moisture divergence over the Bay of Bengal. Such circulation initiates moisture divergence and increases SAT over northern India and the study region (Figures 7a, c). Likewise, the El Niño induces northeasterly wind anomalies during spring and summer, causing positive SAT anomalies and delaying the monsoonal onset (Zhou et al., 2019). Furthermore, the low moisture over

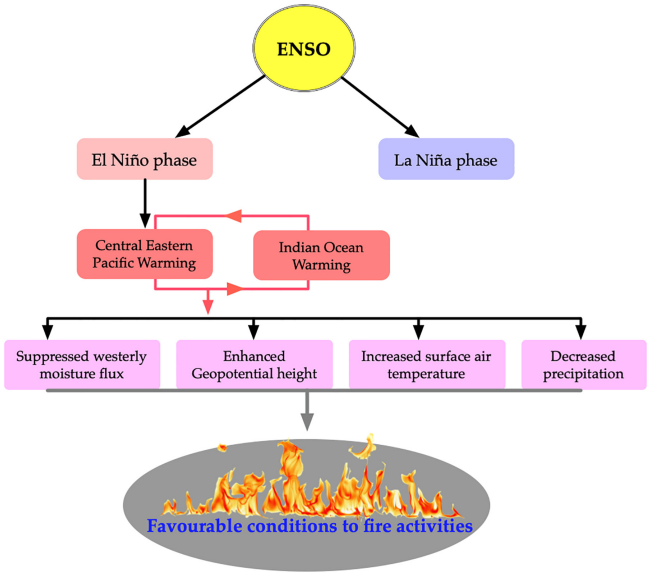

FIGURE 8 Schematic diagram representing linkage of the El Niño with the fire burned areas

India during spring is due to a convergence of strong dry wind that favors the SAT warming (Chowdary et al., 2014). The increased SAT, weakened westerly moisture transport, and abnormal moisture divergence during the El Niño phase resulted in a deficit spring precipitation over the study region (Figure 7d). Overall, these warm and dry condition leads to moisture loss from vegetation, providing more combustible fuels that increase fire activities and fire burned areas.

3.4 | Physical mechanism

Figure 8 presents the significant coupling of the ENSO phase with fire activities; the warming was observed over the central-eastern Pacific Ocean represents the El Niño condition; this enhances the warming of the Indian Ocean in the spring season (Figures 5b, c). It was observed that an anomalous anticyclonic circulation over the southeast Indian Ocean in preceding winter forces warming of the southwest and the north Indian Ocean, creating dry and warm conditions through the northeasterly winds in spring and summer (Zhou et al., 2019). Similarly, high SST anomalies and moisture divergence were observed over the Bay of Bengal during the spring season, producing the northeasterly moisture transport (Figures 5c and 7c). Further, the observed high GPH over the Indian peninsula and Bay of Bengal (Figure 7b) represents the suppressed southerly moisture transport (Fang et al., 2021), which creates warm and dry conditions with reduced precipitation during the El Niño phase (Figures 7a and d). Furthermore, the El Niño phase negatively impacts vegetation health (figure not shown); for instance, the NINO3 in winter and VHI in 2016 were + 2.63 and − 1.22, respectively, indicating that El Niño creates warm and dry conditions to produce the combustible fuel (Figures 4d and 6b). This is consistent with the El Niño impacts on vegetation health due to changes in the surface water inundation, soil moisture, and atmospheric moisture deficits (Du et al., 2021). Overall, these anomalous surface and atmospheric conditions during the El Niño phase provide favorable conditions for fire activities and spread.

4 | CONCLUSIONS

Nepal underwent frequent and severe fire occurrences in recent years with the increased burned areas; affecting human health and well-being, economic assets, biodiversity, atmosphere, and climate. This study attempts to find the climatic and oceanic drivers of the fire burned areas in southern Nepal over the past two decades (2001–2020). The result shows that 91.2% of the fire burned areas only in the spring season, from March to May, with the highest in the month of April. The spring fire burned areas were more-pronounced overlowland areas of the western and central regions. At the interannual timescale, low- precipitation, humidity, soil moisture, and high temperature enhance the evapotranspiration from vegetation, providing more combustible fuels, enhancing the fire activity and spread. In addition, the fire burned areas are significantly linked with the warm phase of ENSO, that is, El Niño in the central-eastern Pacific Ocean in the prior and corresponding seasons. During the El Niño phase, the dry and warm conditions were associated with suppressed westerly moisture transport and abnormal moisture divergence resulting in a deficit of spring precipitation, which induced and enhanced fire activity and burned areas. The present study has mainly focused on the climatic variability associated with wildfires, and we recommend that further study should focus on the anthropogenic influence. The detailed analysis of associated fire driving factors provides essential insight into preparedness, management, and future prediction to limit the multi-dimensional losses in the ecosystem and society.

ACKNOWLEDGEMENTS

The authors would like to express their sincere gratitude to the Department of Hydrology and Meteorology (DHM), Nepal, for providing the station datasets. Scientists at ECMFW and NASA, University of Maryland are also greatly acknowledged for freely providing climatological and active fire datasets.

CONFLICT OF INTEREST

The authors declare that there are no conflicts of interest.

AUTHOR CONTRIBUTIONS

Kalpana Hamal: Data curation; formal analysis; validation; visualization; writing – original draft. **Shravan Kumar Ghimire:** Investigation; writing – review and editing. **Arbindra Khadka:** Writing – review and editing. **Binod Dawadi:** Supervision; writing – review and editing. **Shankar Sharma:** Conceptualization; methodology; validation; visualization; writing – original draft.

DATA AVAILABILITY STATEMENT

The daily data sets for all the stations used in this study can be purchased from DHM, Government of Nepal (http://www.dhm.gov.np/). MODIS active fire detection and burn area products can be freely accessed from https://firms.modaps.eosdis.nasa.gov/download/, and sftp://fuoco.geog.umd.eduserver, respectively. ERA5 gridded datasets used in this study can be freely download from https://cds.climate.copernicus.eu/cdsapp#!/search?type=dataset&text=era5.

ORCID

Kalpana Hamal https://orcid.org/0000-0003-4976-5891
Shravan Kumar Ghimire https://orcid.org/0000-0003-1583-2187
Binod Dawadi https://orcid.org/0000-0001-8263-1356
Shankar Sharma https://orcid.org/0000-0001-7008-5757

REFERENCES

Bartsch, A., Balzter, H. & George, C. (2009) The influence of regional surface soil moisture anomalies on forest fires in Siberia observed from satellites. *Environmental Research Letters*, 4, 045021.

BBC (2021) *Why India and Nepal's forest fires are worrying scientists*. BBC; Avaliable at: https://www.bbc.com/news/world-asia-india-56671148,.

Bhardwaj, P., Naja, M., Kumar, R. & Chandola, H. (2016) Seasonal, interannual, and long-term variabilities in biomass burning activity over South Asia. *Environmental Science and Pollution Research*, 23, 4397–4410.

Bhujel, K.B., Maskey-Byanju, R. & Gautam, A.P. (2017) Wildfire dynamics in Nepal from 2000–2016. *Nepal Journal of Environmental Science*, 5, 1–8.

Bretherton, C.S., Smith, C. & Wallace, J.M. (1992) An intercomparison of methods for finding coupled patterns in climate data. *Journal of Climate*, 5, 541–560.

Burton, C., Betts, R.A., Jones, C.D., Feldpausch, T.R., Cardoso, M. & Anderson, L.O. (2020) El Niño driven changes in global fire 2015/16. *Frontiers in Earth Science*, 8, 199.

C3S. (2017) Copernicus Climate Change Service: ERA5: Fifth generation of ECMWF atmospheric reanalyses of the global climate. Copernicus Climate Change Service Climate Data Store (CDS), November, 2019. https://cds.climate.copernicus.eu/cdsapp#!/home

Carpenter, C. (2005) The environmental control of plant species density on a Himalayan elevation gradient. *Journal of Biogeography*, 32, 999–1018.

Chen, Y., Morton, D.C., Andela, N., Giglio, L. & Randerson, J.T. (2016) How much global burned area can be forecast on seasonal time scales using sea surface temperatures? *Environmental Research Letters*, 11, 045001.

Chen, Y., Morton, D.C., Andela, N., Van Der Werf, G.R., Giglio, L. & Randerson, J.T. (2017) A pan-tropical cascade of fire driven by El Niño/southern oscillation. *Nature Climate Change*, 7, 906–911.

Chen, Y., Sharma, S., Zhou, X., Yang, K., Li, X., Niu, X. et al. (2021) Spatial performance of multiple reanalysis precipitation datasets on the southern slope of central Himalaya. *Atmospheric Research*, 250, 105365. https://doi.org/10.1016/j.atmosres.2020.105365

Chitrakar, G., Piya, B., Nepali, D. & Manandhar, S. (2007) Some notable disasters in Nepal and their mitigation. *Journal of Nepal Geological Society*, 36, 23.

Chowdary, J. & Gnanaseelan, C. (2007) Basin-wide warming of the Indian Ocean during El Niño and Indian Ocean dipole years. *International Journal of Climatology: A Journal of the Royal Meteorological Society*, 27, 1421–1438.

Chowdary, J., John, N. & Gnanaseelan, C. (2014) Interannual variability of surface air-temperature over India: impact of ENSO and Indian Ocean Sea surface temperature. *International Journal of Climatology*, 34, 416–429. https://doi.org/10.1002/joc.3695

Chylek, P., Tans, P., Christy, J. & Dubey, M.K. (2018) The carbon cycle response to two El Nino types: an observational study. *Environmental Research Letters*, 13, 024001.

Curic, M. & Zivanovic, S. (2013) Dependence between deficit and surplus of precipitation and forest fires. *Disaster advances*, 6, 64–69.

Dhakal, S. (2015) Disasters in Nepal. In: *Disaster risk management: concept, policy and practices in Nepal. 05:55 AM" class="old" updatedon="16 Apr, 05:55 AM" mytype="content" id="3140fbfb-aa88-4d3a-94e3-41240d3b13da">,* Kathmandu, Nepal: Central Department of Environmental Science (CDES), Tribhuvan University Kirtipur.

DHM. (2017) Observed climate trend analysis in the districts and physiographic regions of Nepal (1971–2014). *Department of Hydrology and Meteorology, Kathmandu*, 1, 74.

Dong, X., Li, F., Lin, Z., Harrison, S.P., Chen, Y. & Kug, J.-S. (2021) Climate influence on the 2019 fires in Amazonia. *Science of the Total Environment*, 794, 148718.

Du, J., Kimball, J.S., Sheffield, J., Velicogna, I., Zhao, M., Pan, M. et al. (2021) Synergistic satellite assessment of global vegetation health in relation to ENSO-induced droughts and pluvials. *Journal of Geophysical Research: Biogeosciences*, 126, e2020JG006006.

Eskandari, S., Miesel, J.R. & Pourghasemi, H.R. (2020) The temporal and spatial relationships between climatic parameters and fire occurrence in northeastern Iran. *Ecological Indicators*, 118, 106720.

Fang, K., Yao, Q., Guo, Z., Zheng, B., Du, J., Qi, F. et al. (2021) ENSO modulates wildfire activity in China. *Nature communications*, 12, 1–8.

Hamal, K., Sharma, S., Baniya, B., Khadka, N. & Zhou, X. (2020) Inter-annual variability of winter precipitation over Nepal coupled with ocean-atmospheric patterns during 1987–2015. *Frontiers in Earth Science*, 8, 161. https://doi.org/10.3389/feart.2020.00161

Hamal, K., Sharma, S., Pokharel, B., Shrestha, D., Talchabhadel, R., Shrestha, A. et al. (2021) Changing pattern of drought in Nepal and associated atmospheric circulation. *Atmospheric Research*, 262, 105798.

Johnson, E.A. & Miyanishi, K. (2001) Forest fires. In: *Behaviour and ecological effects*. Amsterdam, the Netherlands: Elsevier, p. 570.

Kim, J.-S., Kug, J.-S., Jeong, S.-J., Park, H. & Schaepman-Strub, G. (2020) Extensive fires in southeastern Siberian permafrost linked to preceding Arctic oscillation. *Science advances*, 6, eaax3308.

Kogan, F.N. (2001) Operational space technology for global vegetation assessment. *Bulletin of the American Meteorological Society*, 82, 1949–1964.

Lasko, K. & Vadrevu, K. (2018) Improved rice residue burning emissions estimates: accounting for practice-specific emission factors in air pollution assessments of Vietnam. *Environmental pollution*, 236, 795–806.

Littell, J.S., Peterson, D.L., Riley, K.L., Liu, Y. & Luce, C.H. (2016) Fire and drought [Chapter 7]. In: Vose, J.M., Clark, J.S., Luce, C.H. & Patel-Weynard, T. (Eds.) *Effects of drought on forests and rangelands in the United States: a comprehensive science synthesis. Gen. Tech. Rep. WO-93b*, Vol. 93. Washington, DC: US Department of Agriculture, Forest Service, Washington Office, pp. 135–154.

Lizundia-Loiola, J., Otón, G., Ramo, R. & Chuvieco, E. (2020) A spatio-temporal active-fire clustering approach for global burned area mapping at 250 m from MODIS data. *Remote Sensing of Environment*, 236, 111493.

Mariani, M., Fletcher, M.S., Holz, A. & Nyman, P. (2016) ENSO controls interannual fire activity in Southeast Australia. *Geophysical Research Letters*, 43, 10,891–810,900.

Matin, M.A., Chitale, V.S., Murthy, M.S., Uddin, K., Bajracharya, B. & Pradhan, S. (2017) Understanding forest fire patterns and risk in Nepal using remote sensing, geographic information system and historical fire data. *International journal of wildland fire*, 26, 276–286.

MENRIS-ICIMOD (Ed.). (2008) *Ecology of Nepal*. MENRIS-ICIMOD. Nepal: Internation Centre for Integrated Mountain Development (ICIMOD).

Mishra, V., Smoliak, B.V., Lettenmaier, D.P. & Wallace, J.M. (2012) A prominent pattern of year-to-year variability in Indian summer monsoon rainfall. *Proceedings of the National Academy of Sciences of the United States of America*, 109, 7213–7217. https://doi.org/10.1073/pnas.1119150109

MoHA. 2018. Nepal Disaster Report, 2017; The Road to Sendai. Ministry of Home Affairs, Government of Nepal: Kathmandu, Nepal; 92.

Moinuddin, K., Khan, N. & Sutherland, D. (2021) Numerical study on effect of relative humidity (and fuel moisture) on modes of grassfire propagation. *Fire Safety Journal*, 125, 103422.

Nayava, J.L. (1980) Rainfall in Nepal. *Himalayan Review*, 12, 1–18.

Parajuli, A., Chand, D.B., Rayamajhi, B., Khanal, R., Baral, S., Malla, Y. et al. (2015) *Spatial and temporal distribution of forest fires in Nepal*. Durban, South Africa: In *Proceedings of the XIV World Forestry Congress*.

Perry, L.B., Matthews, T., Guy, H., Koch, I., Khadka, A., Elmore, A. C. et al. (2020) Precipitation characteristics and moisture source regions on Mt. Everest in the Khumbu, Nepal. *One Earth*, 3, 594–607.

Qadir, A., Talukdar, N.R., Uddin, M.M., Ahmad, F. & Goparaju, L. (2021) Predicting forest fire using multispectral satellite measurements in Nepal. *Remote Sensing Applications: Society and Environment*, 23, 100539.

Reddy, C.S., Bird, N.G., Sreelakshmi, S., Manikandan, T.M., Asra, M., Krishna, p.H. et al. (2019) Identification and characterization of spatio-temporal hotspots of forest fires in South Asia. *Environmental Monitoring and Assessment*, 191, 1–17.

Riaz, S.M.F. & Iqbal, M.J. (2017) Singular value decomposition analysis for examining the impact of Siberian high on winter precipitation variability over South Asia. *Theoretical and Applied Climatology*, 130, 1189–1194.

Sharma, S., Hamal, K., Khadka, N. & Joshi, B.B. (2020a) Dominant pattern of year-to-year variability of summer precipitation in Nepal during 1987–2015. *Theoretical and Applied Climatology*, 142, 1071–1084. https://doi.org/10.1007/s00704-020-03359-1

Sharma, S., Hamal, K., Khadka, N., Shrestha, D., Aryal, D. & Thakuri, S. (2021) Drought characteristics over Nepal Himalaya and their relationship with climatic indices. *Meteorological Applications*, 28, e1988.

Sharma, S., Khadka, N., Hamal, K., Shrestha, D., Talchabhadel, R. & Chen, Y. (2020b) How accurately can satellite products (TMPA and IMERG) detect precipitation patterns, extremities, and drought across the Nepalese Himalaya? *Earth and Space Science*, 7, e2020EA001315. https://doi.org/10.1029/2020ea001315

Siegert, F., Ruecker, G., Hinrichs, A. & Hoffmann, A. (2001) Increased damage from fires in logged forests during droughts caused by El Nino. *Nature*, 414, 437–440.

Skamarock, W. (2008) *A description of the advanced research WRF version 3. NCAR Technical Note TN-475+ STR*. Amsterdam, the Netherlands: National Center for Atmospheric Research Boulder. https://www2.mmm.ucar.edu/wrf/users/docs/technote/v3\technote.pdf

Stockwell, I. Introduction to Correlation and Regression analysis. In *Proceedings of the Statistics and Data Analysis. SAS Global Forum*, 2008.

Sungmin, O., Hou, X. & Orth, R. (2020) Observational evidence of wildfire-promoting soil moisture anomalies. *Scientific Reports*, 10, 1–8.

Tang, R., Mao, J., Jin, M., Chen, A., Yu, Y., Shi, X. et al. (2021) Interannual variability and climatic sensitivity of global wildfire activity. *Advances in Climate Change Research*, 12, 686–695.

Tanoue, M., Ichiyanagi, K., Yoshimura, K., Kiguchi, M., Terao, T. & Hayashi, T. (2018) Seasonal variation in isotopic composition and the origin of precipitation over Bangladesh. *Progress in Earth and Planetary Science*, 5, 1–16.

Thornthwaite, C.W. (1948) An approach toward a rational classification of climate. *Geographical review*, 38, 55–94.

Upreti, B. (2001) The physiographic and geology of Nepal and their bearing on the landslide problem. *Landslide hazard mitigation in the Hindu Kush-Himalaya*, 7, 31–49.

Vadrevu, K. P. (2016) Vegetation fires and air pollution in South/Southeast Asia–Analysis from multi-satellite datasets. In NASA/UAH Earth and Atmospheric Science Seminar (No. MSFC-E-DAA-TN35857). Accessed from: https://www.nies.go.jp/soc/en/events/iwggms9/pdf/presentations/0531/30_KrishnaVadrevu.pdf

Vadrevu, K.P., Lasko, K., Giglio, L., Schroeder, W., Biswas, S. & Justice, C. (2019) Trends in vegetation fires in south and southeast Asian countries. *Scientific Reports*, 9, 1–13.

Vicente-Serrano, S.M., Beguería, S. & López-Moreno, J.I. (2010) A multiscalar drought index sensitive to global warming: the standardized precipitation evapotranspiration index. *Journal of Climate*, 23, 1696–1718. https://doi.org/10.1175/2009jcli2909.1

Wang, G. & Cai, W. (2020) Two-year consecutive concurrences of positive Indian Ocean dipole and Central Pacific El Niño preconditioned the 2019/2020 Australian "black summer" bushfires. *Geoscience Letters*, 7, 1–9.

Wang, S.H., Lin, N.H., Chou, M.D. & Woo, J.H. (2007) Estimate of radiative forcing of Asian biomass-burning aerosols during the period of TRACE-P. *Journal of Geophysical Research: Atmospheres*, 112(D10). https://doi.org/10.1029/2006JD007564

Yang, Y., Wu, L., Guo, Y., Gan, B., Cai, W., Huang, G. et al. (2021) Greenhouse warming intensifies north tropical Atlantic climate variability. *Science advances*, 7, eabg9690.

Yi, K., Bao, Y. & Zhang, J. (2017) Spatial distribution and temporal variability of open fire in China. *International journal of wildland fire*, 26, 122–135.

Zhao, F. & Liu, Y. (2019) Atmospheric circulation patterns associated with wildfires in the monsoon regions of China. *Geophysical Research Letters*, 46, 4873–4882.

Zhongming, Z., Linong, L., Wangqiang, Z. and Wei, L. (2021) Fires ravage forests in Himalayas, threatening health and biodiversity.

Zhou, Z.-Q., Zhang, R. & Xie, S.-P. (2019) Interannual variability of summer surface air temperature over Central India: implications for monsoon onset. *Journal of Climate*, 32, 1693–1706. https://doi.org/10.1175/JCLI-D-18-0675.1

SUPPORTING INFORMATION

Additional supporting information may be found in the online version of the article at the publisher's website.

How to cite this article: Hamal, K., Ghimire, S. K., Khadka, A., Dawadi, B., & Sharma, S. (2022). Interannual variability of spring fire in southern Nepal. *Atmospheric Science Letters*, *23*(9), e1096. https://doi.org/10.1002/asl.1096